ACS NANO

www.acsnano.org

ARTICLE

Plant Cell Wall-Inspired Interfacial Bridging Enables Ultrastrong and Tough Carbon Nanotube Fibers

Xiangyang Li, Xudong Lei, Xiangzheng Jia, Muqiang Jian,* Tongzhao Sun, Xinyin Yang, Jiankun Huang, Xiaocang Han, Haolu Lin, Yunhang Li, Jiajun Luo, Xiaoxu Zhao, Enlai Gao, Xianqian Wu, and Jin Zhang*

Cite This: https://doi.org/10.1021/acsnano.5c14235

Read Online

ACCESS | Metrics & More | Article Recommendations | Supporting Information

ABSTRACT: Achieving simultaneous enhancement of strength and toughness in carbon nanotube fibers (CNTFs) remains a persistent challenge due to inefficient interfacial load transfer, low nanotube alignment, and high porosity. Herein, inspired by the hierarchical architecture and borate-mediated cross-linking of plant cell walls, we report a bioinspired interfacial bridging strategy to fabricate ultrastrong and tough CNTFs. This approach involves the sequential infusion of poly(pyridobisimidazole) (PIPD) nanofibers and chains into CNTF networks, followed by borate-induced covalent cross-linking and mechanical densification. The PIPD molecular backbone consists of alternating pyridobisimidazole and dihydroxyphenyl rings, which enable the formation of hydrogen bonding and borate-mediated covalent cross-linking network with CNTs. The resulting fibers exhibit strong intertube interactions, improved alignment, and reduced porosity. Consequently, CNTFs achieve an ultrahigh tensile strength of 8.45 ± 0.28 GPa and a high toughness of 238.42 ± 14.78 MJ·m^{-3}, surpassing the performance of commercial high-performance fibers. Additionally, the fibers exhibit high impact resistance with a specific penetration energy of 1.26 MJ·kg^{-1}, outperforming many state-of-the-art protective materials. Experimental characterizations combined with first-principles calculations reveal that the synergistic interplay between the highly ordered assembly and strengthened interfacial interactions enables cooperative deformation and efficient energy dissipation. This work establishes a scalable and biomimetic pathway for fabricating CNTFs with a combination of ultrahigh strength and toughness, making them promising candidates for advanced structural and protective applications.

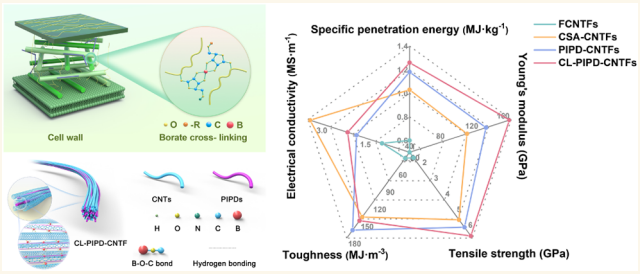

KEYWORDS: *bioinspired, carbon nanotube fibers, strength, toughness, interfacial bridging, impact-resistant*

INTRODUCTION

Simultaneously elevating the strength and toughness of fiber materials remains an enduring challenge, particularly for advanced protective systems exposed to high-strain-rate and ballistic conditions. In synthetic fibers, these two mechanical properties are often mutually exclusive due to inherent structural trade-offs in material design.[1] In contrast, natural materials have evolved hierarchical architectures that effectively reconcile strength with toughness, frequently surpassing their synthetic counterparts.[2,3] Wood exemplifies this natural design strategy. Its cell walls provide sufficient strength and stiffness to sustain macroscopic loads while remaining sufficiently extensible to accommodate cellular growth. These attributes originate from a hierarchical assembly of cellulose, hemicellulose, and lignin.[4−11] Cellulose chains assemble into densely packed nanofibrils, where the highly ordered crystalline domains of cellulose confer excellent intrinsic strength.[5,12,13] These nanofibrils are highly aligned along the longitudinal axis of cell walls, contributing to the macroscopic strength of wood.[14] The nanofibrils are embedded in a hemicellulose and lignin matrix that provides additional reinforcement through robust interfacial interactions.[11,12,15] Notably, borate-mediated covalent cross-links between rhamnogalacturonan II side chains significantly enhance the interfacial cohesion (Figure 1a), enabling efficient energy dissipation and conferring both

Received: August 20, 2025
Revised: December 14, 2025
Accepted: December 16, 2025

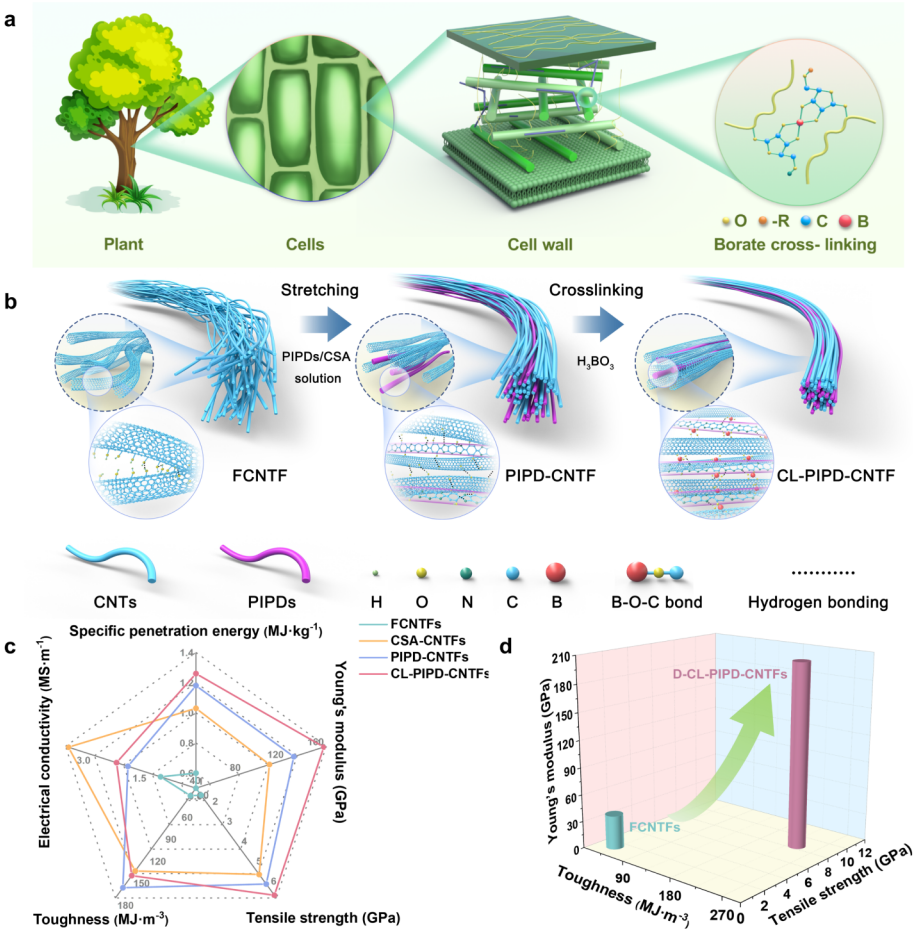

Figure 1. Fabrication and performance of CNTFs. (a) Schematic illustration of the hierarchical structure and borate-mediated cross-linking found in plant cell walls, which collectively confer high strength and toughness. (b) Schematic diagram of the fabrication of CL-PIPD-CNTFs involving sequential interfacial bridging via hydrogen bonding and borate-mediated covalent bonding. (c) Comparison of the mechanical and electrical performance of different CNTFs. (d) Comparison of the mechanical properties of FCNTFs and D-CL-PIPD-CNTFs.

high strength and toughness to the material.[16] This natural design paradigm suggests that mimicking the high-performance building blocks, hierarchical organization, and interfacial bridging of plant cell walls offers a promising strategy for constructing fiber materials that concurrently achieve superior strength and toughness.

Carbon nanotubes (CNTs) are widely regarded as one of the strongest and toughest known materials, with an intrinsic tensile strength reaching 120 GPa and a toughness approaching 8 GJ·m^{-3}.[17] These exceptional properties stem from their unique sp^2 -bonded carbon lattice and one-dimensional nanostructured morphology, making them ideal nanoscale building blocks for next-generation high-performance fibers.[18,19] However, the mechanical performances of macroscopic CNT fibers (CNTFs) remain significantly inferior to those of individual CNTs, primarily due to the structural limitations arising from the assembly process. These include weak interfacial interactions, poor nanotube alignment, and high porosity, which collectively compromise efficient load transfer from individual CNTs to CNTFs and energy dissipation.[20−23] To address these issues, extensive efforts have focused on tailoring the hierarchical architecture of CNTFs through a range of processing strategies. These include optimization of spinning parameters,[24,25] axial stretching,[26−30] mechanical densification,[31−33] thermal annealing,[34,35] and reinforcement of intertube interactions.[36−41] While each of these approaches contributes to improvements in strength or toughness, achieving concurrent enhancement of both properties remains elusive. Recently, we developed an integrated strategy combining progressive axial stretching, polymer infusion, and mechanical densification to simultaneously enhance interfacial interactions, nanotube alignment, and fiber densification.[42] This process yielded fibers with significantly improved tensile strength and offers a viable route toward the fabrication of high-performance CNTFs. Further advances in mechanical performance are essential for meeting the stringent demands of advanced structural and protective applications.

As one of the most advanced high-performance polymers, poly(pyridobisimidazole) (PIPD) fibers exhibit exceptional tensile strength, high modulus, and good thermal and chemical stability.[43,44] These properties originate from its rigid molecular backbone, which consists of alternating pyridobisimidazole and dihydroxyphenyl rings that promote extensive intra- and intermolecular hydrogen bonding networks.[45,46] When integrated with functionalized CNTs, these hydroxyl groups act as active sites for forming both hydrogen bonding and borate-mediated covalent cross-linking networks, generating a tightly coupled hybrid interface that markedly enhances load transfer and structural integrity. Herein, drawing

https://doi.org/10.1021/acsnano.5c14235
ACS Nano XXXX, XXX, XXX−XXX

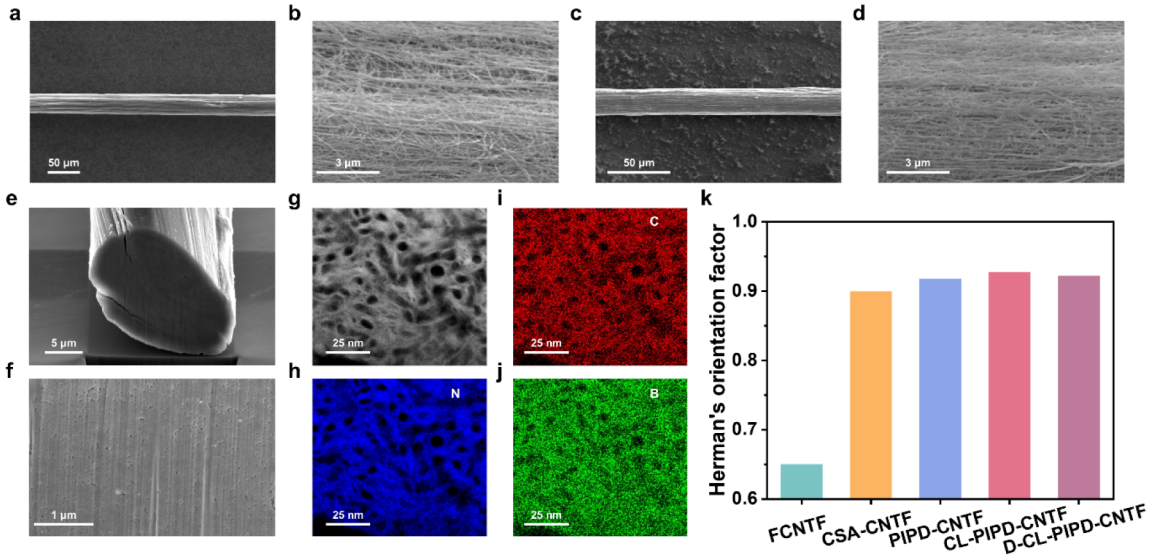

Figure 2. Structural characterization of CNTFs. (a, b) SEM images of FCNTFs. (c, d) SEM images of CL-PIPD-CNTFs. (e, f) Cross-sectional SEM images of CL-PIPD-CNTFs prepared by a focused ion beam (FIB). (g) HAADF-STEM image of the radial cross-section of CL-PIPD-CNTFs. (h–j) Corresponding elemental mappings of nitrogen (N), carbon (C) and boron (B). (k) Comparison of Herman's orientation factors for different fibers.

inspiration from the hierarchically ordered architecture and borate-mediated cross-linking of plant cell walls, we present a biomimetic strategy for the fabrication of ultrastrong and tough CNTFs. This strategy involves the infusion of poly(pyridobisimidazole) (PIPD) nanofibers and chains (PIPDs), followed by the introduction of borate ions and mechanical densification. In this fiber system, the highly aligned CNTs, analogous to cellulose nanofibrils, serve as the primary reinforcing skeleton, while the PIPDs emulate the hemicellulose/lignin matrix by forming both hydrogen bonding and borate-mediated covalent cross-linking with the CNT network. This dual-bonding mechanism enhances intertube cohesion and facilitates efficient load transfer, resulting in a well-balanced combination of strength and toughness. The CNTFs exhibit a high tensile strength of 8.45 ± 0.28 GPa and a remarkable toughness of 238.42 ± 14.78 MJ·m^{-3}, along with high specific penetration energy, highlighting their potential for advanced impact-resistant applications. Spectroscopic analyses, stress relaxation experiments, and first-principles calculations reveal that enhanced interfacial interactions, improved nanotube alignment, and reduced porosity, collectively account for the superior mechanical performance.

RESULTS AND DISCUSSION

Fabrication and Structural Characterization of CNTFs. Figure 1b illustrates the fabrication process of interfacial-bridging-enabled ultrastrong and tough CNTFs. Functionalized CNTFs (FCNTFs), bearing oxygen-containing functional groups (e.g., hydroxyl groups), are first immersed in a chlorosulfonic acid (CSA) solution containing PIPDs. During the axial stretching process, PIPDs are infused into the CNTF network, forming a hydrogen bonding network and yielding highly aligned, densified PIPD-modified CNTFs (PIPD-CNTFs). As a control, FCNTFs are also axially stretched in neat CSA to produce CSA-treated CNTFs (CSA-CNTFs). Subsequent intercalation of borate ions into PIPD-CNTFs induces robust interfacial bridging through the covalent cross-linking between CNTs and PIPDs, forming cross-linked fibers (CL-PIPD-CNTFs). This hierarchically ordered architecture imparts significantly enhanced mechanical performance compared to FCNTFs, CSA-CNTFs, and PIPD-CNTFs. A final mechanical rolling treatment further densifies the fibers, resulting in D-CL-PIPD-CNTFs. These fibers exhibit an ultrahigh tensile strength of 8.45 ± 0.28 GPa, a remarkable toughness of 238.42 ± 14.78 MJ·m^{-3}, a high Young's modulus of 203.99 ± 8.66 GPa, and an electrical conductivity of 2.60 MS·m^{-1}, which are 5.3, 4.9, 4.4, and 1.5 times increases over those of FCNTFs, respectively (Figure 1c,d).

We systematically investigated the structural evolution of CNTFs throughout each stage of the optimization process. Raw CNTFs, primarily composed of multiwalled CNTs (Figure S1), were synthesized by floating catalyst chemical vapor deposition as previously reported.[32,42] A subsequent purification process involving mild oxidation and acid washing effectively removed residual impurities (e.g., metallic catalyst particles and amorphous carbon), and introduced hydroxyl groups onto the CNT surfaces, yielding FCNTFs. Thermogravimetric analysis, Raman spectroscopy, and X-ray photoelectron spectroscopy (XPS) confirm the successful removal of impurities and the introduction of oxygen-containing groups on the CNTs (Figure S2). Despite these modifications, the as-purified FCNTFs retain a disordered architecture with loosely entangled CNTs and a high density of voids (Figure 2a,b, and Figure S3). To improve nanotube alignment and structural packing, FCNTFs were swollen in CSA, leveraging sidewall protonation effects, and subjected to axial stretching. The resulting CSA-CNTFs exhibit a more aligned and compact network, resulting in improved tensile strength and toughness relative to FCNTFs (Figures S4 and S5). Nonetheless, voids remained present in the CSA-CNTFs (Figure S6), limiting further mechanical enhancement. To mitigate this, PIPDs were infused into FCNTFs during the axial stretching process by dissolving PIPD fibers in a CSA solution, producing PIPD-CNTFs (Figure S7). Three kinds of PIPD-CNTFs with different weight percent (wt %) of PIPDs were fabricated.

https://doi.org/10.1021/acsnano.5c14235
ACS Nano XXXX, XXX, XXX−XXX

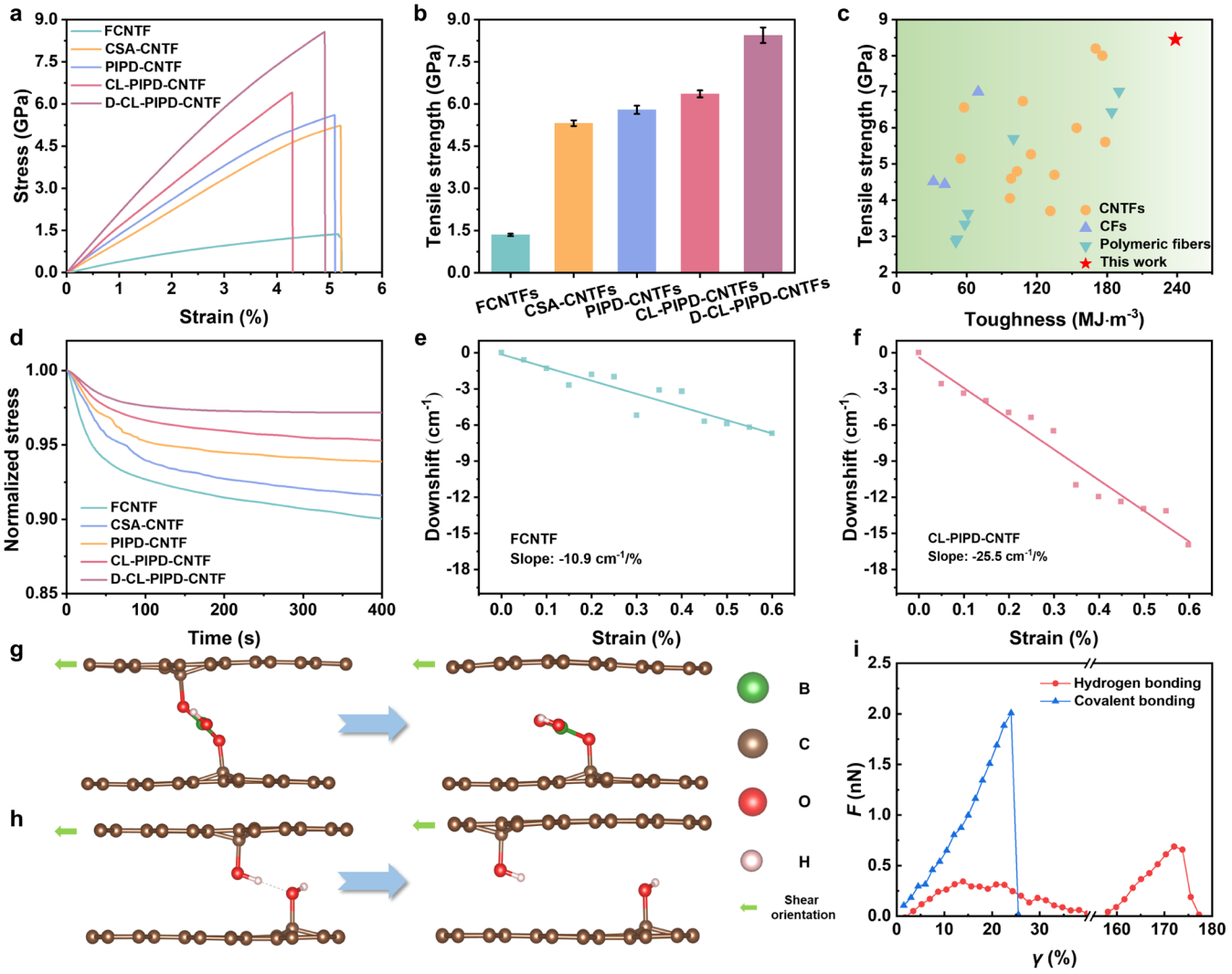

Figure 3. Mechanical performance and reinforcement mechanism of CNTFs. (a) Representative stress−strain curves of FCNTFs, CSA-CNTFs, PIPD-CNTFs, CL-PIPD-CNTFs, and D-CL-PIPD-CNTFs. (b) Comparison of tensile strength of different CNTFs. (c) Comparison of the tensile strength and toughness of the present CNTFs and other state-of-the-art high-performance fibers. (d) Stress-relaxation curves of different fibers at 1.5% strain. (e, f) Dependence of Raman frequency downshifts on the applied strains for FCNTFs and CL-PIPD-CNTFs. (g, h) Atomistic simulations of interfacial structures with borate-mediated covalent bonding and hydrogen bonding before and after shear loading. (i) Shear force-shear strain curves interfacial structures with borate-mediated covalent bonding and hydrogen bonding in CNTFs.

Among them, PIPD-CNTFs treated in the solution with a PIPDs concentration of 0.1 wt % exhibit the highest PIPDs content (Table S1) and superior tensile strength (Figure S8 and Table S2). Surface and cross-sectional scanning electron microscopy (SEM) images reveal fewer voids in these fibers (Figure S9a−d), while energy-dispersive spectroscopy (EDS) mappings confirm the homogeneous distribution of carbon, oxygen, and nitrogen, indicating uniform incorporation of PIPDs across the fiber cross sections (Figure S9e−h). To further strengthen interfacial interactions, borate ions were subsequently introduced to establish strong interfacial bridging between CNTs and PIPDs inspired by the borate-mediated cross-linking chemistry in plant cell walls, forming CL-PIPD-CNTFs. To identify the optimal concentration of borate ions, three concentrations were tested, and the highest tensile strength was achieved with a borate concentration of 1 g·L^{-1} (Figure S10 and Table S3). At this optimal concentration, three kinds of fibers were fabricated with different immersion durations. CL-PIPD-CNTFs produced with an immersing duration of 12 h exhibit the highest tensile strength (Figures S11, S12, and Table S4). Surface and cross-sectional SEM images (Figure 2c−f), and high-angle annular dark-field scanning transmission electron microscopy (HAADF-STEM) images (Figure 2g) confirm a highly aligned and densely packed CNT architecture in CL-PIPD-CNTFs. Elemental mappings of carbon, nitrogen, and boron further validate the uniform distribution of PIPDs and borate cross-linkers throughout the fiber cross sections (Figure 2h−j). Finally, mechanical rolling was further applied to densify the fibers, yielding D-CL-PIPD-CNTFs with enhanced structural integrity and tensile strength (Figures S13 and S14).

We systematically evaluated the effects of axial stretching and interfacial bridging on nanotube alignment, structural densification, and interfacial interactions in CNTFs. Wide-angle X-ray scattering (WAXS) patterns and corresponding azimuthal intensity profiles of different fibers reveal progressively enhanced alignment in CSA-CNTFs, PIPD-CNTFs, CL-PIPD-CNTFs, and D-CL-PIPD-CNTFs relative to pristine

https://doi.org/10.1021/acsnano.5c14235
ACS Nano XXXX, XXX, XXX−XXX

FCNTFs (Figure S15). Herman's orientation factors, derived from WAXS data, increased from 0.650 in FCNTFs to 0.900, 0.918, 0.927, and 0.922 in CSA-CNTFs, PIPD-CNTFs, CL-PIPD-CNTFs, and D-CL-PIPD-CNTFs, respectively (Figure 2k), indicating substantial improvement in nanotube alignment along the fiber axis. Small-angle X-ray scattering (SAXS) was employed to assess nanoscale structural densification. Equatorial scattering intensity profiles exhibit markedly reduced intensity for D-CL-PIPD-CNTFs (Figure S16), indicative of diminished electron density contrast between CNTs and voids, consistent with higher packing density. These observations align with cross-sectional SEM images (Figure 2e,f). To elucidate the interfacial interactions, Fourier transform infrared spectroscopy (FTIR) and XPS were conducted. In FTIR spectra, the stretching band of the hydroxyl group at 3463 cm^{-1} in FCNTFs exhibits a redshift to 3393 cm^{-1} in PIPD-CNTFs, reflecting hydrogen bonding between CNTs and PIPDs (Figure S17a).[47−49] Upon borate ions intercalation, a characteristic B−O−C stretching band at 1125 cm^{-1} emerges, consistent with covalent cross-linking.[48,50] A further redshift of the stretching band of the hydroxyl group in CL-PIPD-CNTFs suggests a strengthened hydrogen bonding network. XPS spectra confirm the successful incorporation of borate ions, as evidenced by the appearance of a distinct B 1s peak at ∼192 eV in CL-PIPD-CNTFs (Figure S17b),[49,51] which is absent in PIPD-CNTFs. These results demonstrate that this bioinspired interfacial bridging strategy significantly enhances nanotube alignment, structural densification, and interfacial interactions within CNTFs.

Performance and Enhancement Mechanism of CNTFs. The synergistic enhancement of nanotube alignment, structural densification, and interfacial interactions contributes to the superior mechanical and electrical performance of the resulting fibers. D-CL-PIPD-CNTFs achieve a high tensile strength of 8.45 ± 0.28 GPa (Figure 3a,b), which is 6.3, 1.6, 1.5, and 1.3 times that of FCNTFs (1.35 ± 0.04 GPa), CSA-CNTFs (5.32 ± 0.10 GPa), PIPD-CNTFs (5.80 ± 0.15 GPa), and CL-PIPD-CNTFs (6.36 ± 0.12 GPa) (Table S5), respectively. In addition to high strength, D-CL-PIPD-CNTFs also exhibit an ultrahigh toughness of 238.42 ± 14.78 $MJ{\cdot}m^{-3}$, representing a 4.9-fold greater than that of FCNTFs. These results demonstrate good internal consistency, as supported by the 95% confidence intervals and significance testing (at the significance level of 0.05). This unprecedented combination of high strength and toughness surpasses those of commercial carbon and polymeric fibers, as well as state-of-the-art CNTFs reported to date (Figure 3c and Table S6).[28,52−56] Additionally, CSA-CNTFs exhibit an electrical conductivity of 3.42 $MS{\cdot}m^{-1}$, which is 2.6 times increase over that of FCNTFs. This contributes to the pronounced improvements in nanotube alignment and structural compactness of CSA-CNTFs. Despite the introduction of polymer components, D-CL-PIPD-CNTFs maintain a high electrical conductivity of 2.60 $MS{\cdot}m^{-1}$, exceeding those of MXene,[57] graphene,[58] and conventional carbon fibers.[59]

To understand the strengthening mechanism, we conducted stress relaxation and in situ Raman spectroscopy experiments, as well as atomistic simulations. In FCNTFs, weak intertube interactions and structural defects facilitate nanotube slippage during deformation, resulting in low relaxation resistance, with ∼90% of the initial stress retained after relaxation at 1.5% strain (Figure 3d). In contrast, CL-PIPD-CNTFs exhibit markedly enhanced resistance to stress relaxation due to improved interfacial bonding and compact nanotube packing, which effectively suppresses slippage of nanotubes. D-CL-PIPD-CNTFs demonstrate the highest resistance, retaining 97.5% of the initial stress under the same conditions. To further probe load-transfer efficiency, in situ Raman spectroscopy was performed. The G′-band shift under strain serves as a quantitative indicator of stress transfer across the nanotube network.[38] FCNTFs show a modest shift of −10.9 cm^{-1} under the tensile strain (Figure 3e), which is consistent with their inefficient stress transfer and inferior mechanical properties. Intermediate shifts observed for CSA-CNTFs and PIPD-CNTFs confirm a gradual enhancement in load-transfer efficiency (Figure S18a,b), aligning with their improved tensile strength and toughness. CL-PIPD-CNTFs and D-CL-PIPD-CNTFs exhibit pronounced downshifts of −25.5 and −29.7 cm^{-1} (Figure 3f and Figure S18c), respectively, suggesting strong interfacial bridging and efficient load distribution across the network. Notably, the G′-band shift per unit strain in CL-PIPD-CNTFs and D-CL-PIPD-CNTFs is more than twice that of FCNTFs, further substantiating the effectiveness of the bioinspired interfacial bridging strategy in enhancing mechanical properties. To further understand the strengthening mechanism, we did first-principles calculations. The incorporation of borate ions facilitates covalent cross-linking between hydroxyl groups on PIPDs and CNTFs, resulting in the formation of borate-mediated covalent bonding (Figure 3g). To quantify the mechanical performance of these interfacial bridges, we computed the shear force (F)-strain (γ) responses of both borate-mediated covalent bonding and typical hydrogen bonding in CNTFs (Figure 3h, i). Borate-mediated covalent bonding exhibits a significantly higher interfacial shear strength (2.01 nN) and critical shear strain (24%) compared to the hydrogen bonding (0.34 nN and 14%). For comparison, the shear strength per atom for van der Waals interactions is only 8.68 pN (Figure S19), much lower than that of either borate-mediated covalent bonding or hydrogen bonding. Meanwhile, the hydrogen bonding exhibits dynamic reversibility (Figure 3i). The synergistic interplay between the strong, stiff borate-mediated covalent bonding and reversible, ductile hydrogen bonding contributes to the strong and tough interfacial interactions and thus the mechanical performance of CL-PIPD-CNTFs and D-CL-PIPD-CNTFs.

In assemblies with poor load-transfer efficiency, individual CNTs are easily pulled out from bundles under applied stress. In contrast, architectures with strong intertube interactions promote cooperative deformations, with load shared across neighboring nanotubes, leading to extension rather than slippage. This distinction in failure morphology highlights the critical role of interfacial bridging in enabling effective stress transfer throughout the fibers. Fractographic analysis reveals that FCNTFs predominantly fail via intertube slippage, characterized by abundant pulled-out bundles, whereas CL-PIPD-CNTFs exhibit significantly fewer pulled-out bundles upon fracture (Figure S20), indicating reinforced intertube cohesion. These observations confirm that the bioinspired interfacial bridging strategy significantly enhances nanotube alignment, structural densification, and interfacial load transfer, synergistically contributing to the high tensile strength and toughness of the resulting fibers.

Specific Penetration Energy of CNTFs. Beyond their quasi-static mechanical performance, the impact resistance of CNTFs was directly assessed using laser-induced microbullet impact testing. In this setup, microbullets (with an average

https://doi.org/10.1021/acsnano.5c14235
ACS Nano XXXX, XXX, XXX−XXX

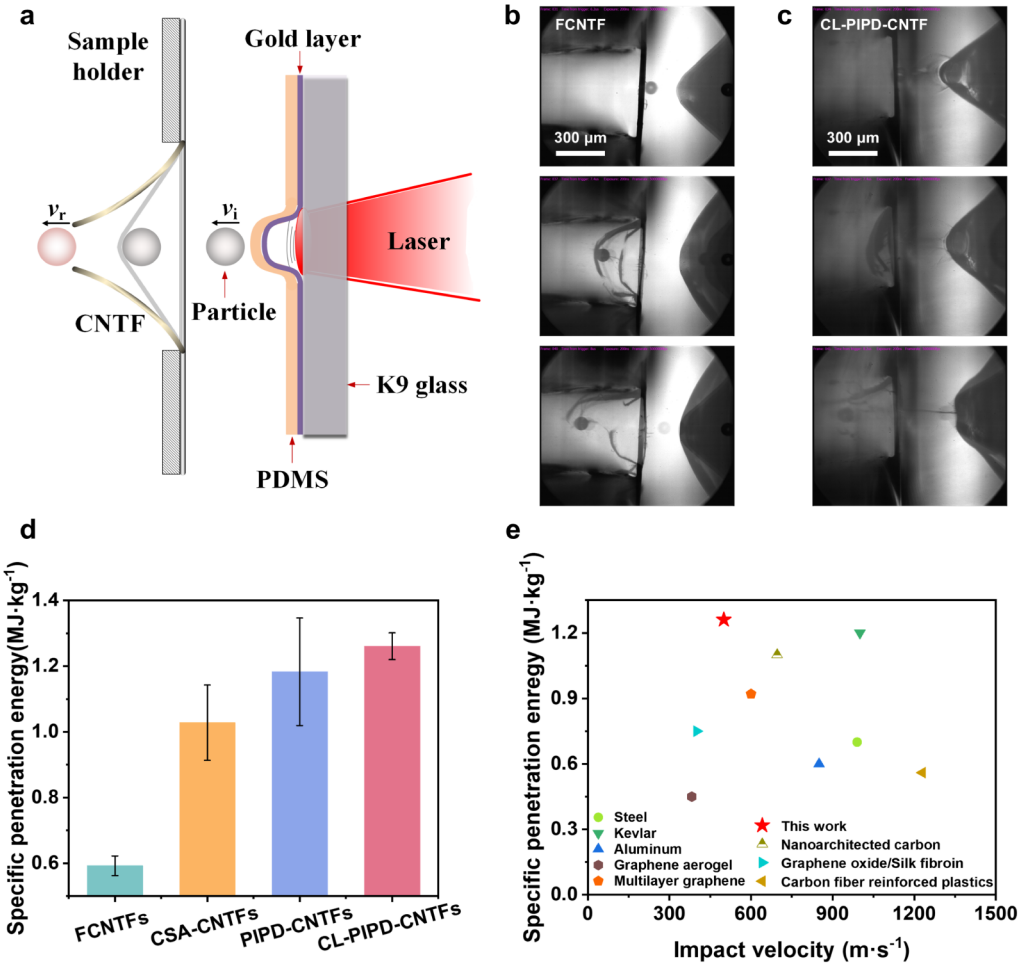

Figure 4. Specific penetration energy of CNTFs. (a) Schematic diagram of laser-induced microbullet impact on a fiber. Here, v_i and v_r represent the impact and residual velocity of the microbullet, and PDMS denotes the polydimethylsiloxane. (b, c) Time-resolved digital images capturing microbullet impact and penetration processes in an FCNTF and a CL-PIPD-CNTF. (d) Comparison of specific penetration energy for different CNTFs. (e) Specific penetration energy of CL-PIPD-CNTFs compared to commercial and reported high-performance materials.

diameter of 98.62 ± 4.06 μm) were accelerated to an average velocity of about 500 m·s^{-1}, impacting an individual fiber (Figure 4a). The velocities before and after fiber penetration are recorded via high-speed imaging to calculate the specific penetration energy. Time-resolved images of the impact and penetration processes for FCNTFs and CL-PIPD-CNTFs are shown in Figure 4b,c. CL-PIPD-CNTFs exhibit the highest specific penetration energy of 1.26 MJ·kg^{-1}, representing a 1.1-fold increase over FCNTFs (Figure 4d). This value is comparable to, or exceeds, those reported for other advanced energy-absorbing nanomaterials, such as graphene aerogels[60] and pyrolyzed carbon nanolattices.[61] Notably, the performance surpasses that of traditional impact-resistant materials such as steel, aluminum, and Kevlar armor (Figure 4e and Table S7).[62,63] This superior impact resistance, reflecting their excellent dynamic mechanical robustness, is attributed to the highly ordered architecture and robust interfacial interactions within the fiber network,[39,42,54] which enable a greater fraction of CNTs to engage in load-bearing under dynamic loading. This facilitates stress-induced bond rupture and potential atomic rearrangement, enhancing energy dissipation efficiency.[42,64] These findings underscore the exceptional impact resistance of CNTFs and suggest their promise for applications in advanced armor systems, protective textiles, and blast-resistant structural materials.

CONCLUSIONS

Drawing inspiration from the hierarchical architecture and interfacial chemistry of plant cell walls, we present an interfacial bridging strategy for engineering ultrastrong and tough CNTFs through sequential infusion of PIPDs, borate-mediated covalent cross-linking, and mechanical densification. This bioinspired strategy simultaneously enhances nanotube alignment, structural densification, and interfacial interactions. The resulting D-CL-PIPD-CNTFs exhibit exceptional tensile strength (8.45 ± 0.28 GPa) and ultrahigh toughness (238.42 ± 14.78 MJ·m^{-3}). Additionally, the fibers demonstrate superior impact resistance with a specific penetration energy of 1.26 MJ·kg^{-1}. Comprehensive structural, spectroscopic, mechanical analyses, and simulations reveal that interfacial bridging plays a pivotal role in suppressing slippage of nanotubes, enabling cooperative deformation and efficient energy dissipation under both quasi-static and dynamic loading. These findings establish a robust and biomimetic design principle for high-performance CNTFs, and offer a promising route toward next-generation protective materials for use in advanced armor, textiles, and

https://doi.org/10.1021/acsnano.5c14235
ACS Nano XXXX, XXX, XXX−XXX

blast-resistant systems. There remain certain limitations to the large-scale production and practical application of these fibers. The current structural optimization process still relies on CSA and acetone as processing solvents, which raises concerns regarding environmental impact and industrial scalability. Moreover, the interfacial-bridging procedure is relatively time-consuming. Future efforts should focus on developing greener solvent systems and simplifying the overall fabrication process to improve sustainability and production efficiency.

EXPERIMENTAL SECTION

Preparation of Raw CNTFs. The raw CNTFs were prepared by the floating catalyst chemical vapor deposition method.[30,32] A precursor solution consisting of acetone as the liquid carbon source, with dissolved ferrocene (Aladdin, 99%) and thiophene (Aladdin, 99%) as catalyst and promoter, respectively, was injected into the reactor at a rate of 30 mL·h^{-1}. The solution was transported into the high-temperature zone (1300 °C) by a carrier gas mixture of hydrogen and argon (5 L·min^{-1}). Within the reaction zone, CNTs nucleated and self-assembled into hollow, cylinder-like aerogels. As the aerogels exited the reactor, they passed through a water bath, forming continuous CNTFs, which were subsequently collected on a bobbin at a winding rate of ∼15 m·min^{-1}. The as-spun CNTFs were then dried at 400 °C to remove residual moisture and stabilize the structure.

Preparation of FCNTFs. The as-spun CNTFs were first treated with a 30% hydrogen peroxide solution (Macklin) at room temperature for 12 h to remove amorphous carbon and introduce oxygen-containing functional groups. The obtained fibers were then rinsed thoroughly with deionized water and subsequently immersed in an acidic solution for 3 h to eliminate residual iron catalyst particles. Afterward, the CNTFs were washed three times with deionized water and dried in an oven at 70 °C under an air atmosphere to remove residual moisture, yielding FCNTFs.

Preparation of CSA-CNTFs. FCNTFs were first immersed in a CSA solution (Aladdin, 99.5%). Subsequently, they were subjected to axial stretching to improve the nanotube alignment. Following stretching, the CSA-CNTFs were transferred into an acetone bath (Aladdin, 99%) to remove residual CSA and induce structural densification.

Preparation of PIPD-CNTFs. PIPD fibers (provided by China Bluestar Chengrand Research Institute of Chemical Industry) were dissolved and dispersed in CSA at concentrations of 0.05, 0.1, and 0.2 wt %, respectively. The mixtures were stirred for 6 h at room temperature to obtain the homogeneous PIPD dispersions. FCNTFs were then immersed in the dispersions and subjected to axial stretching to promote nanotube alignment and interfacial interaction. During the drawing process, the fibers were immersed in the dispersions and stretched axially with a draw ratio of about 20% at room temperature for 10 min. The treated fibers were subsequently transferred into an acetone (Aladdin, 99%) bath to remove CSA and dried overnight at room temperature to obtain PIPD-CNTFs.

Preparation of CL-PIPD-CNTFs. Boric acid (Aladdin, 99.5%) was dissolved in the deionized water at concentrations of 0.5, 1, and 2 g·L^{-1}. After the dissolution of boric acid, the pH of above solutions was adjusted to 8 through NaOH (Aladdin, 96%). The as-prepared PIPD-CNTFs were then immersed in these borate solutions for 12 h at room temperature to induce cross-linking. After treatment, the fibers were rinsed three times with deionized water and annealed at 90 °C under vacuum for 4 h to yield CL-PIPD-CNTFs.

Preparation of D-CL-PIPD-CNTFs. To further enhance the packing density, a mechanical densification process was applied using a roller press (MSK-2150, SHENZHEN KEJINGSTAR Technology Company, Ltd., China). Before rolling, the resulting CL-PIPD-CNTFs were sandwiched between two aluminum foils (KLBIO, 10 μm thick). The roller gap was adjusted to eliminate visible spacing, and the fibers were rolled under these conditions. The rolling process compacted the fiber structure, yielding D-CL-PIPD-CNTFs.

ASSOCIATED CONTENT

Supporting Information

The Supporting Information is available free of charge at https://pubs.acs.org/doi/10.1021/acsnano.5c14235.

Experimental methods: WAXS, SAXS, quasi-static mechanical properties, stress relaxation measurements, first-principles calculations, and other characterizations; stress−strain plots, TEM, TGA, XPS, Raman, SEM of FCNTFs and CSA-CNTFs; TEM, HRTEM, EDS of PIPDs; stress−strain curves of fibers treated with PIPD concentration; SEM, STEM, and EDS of PIPD-CNTFs; stress−strain curves of fibers treated with different boric acid concentrations and times; SEM, stress−strain curves of CL-PIPD-CNTFs and D-CL-PIPD-CNTFs; WAXS, SAXS, FTIR, and in situ Raman of different fibers; simulation of van der Waals interaction and fracture morphologies of different fibers (PDF)

AUTHOR INFORMATION

Corresponding Authors

Muqiang Jian − *Beijing Graphene Institute (BGI), Beijing 100095, China*; Email: jianmq-cnc@pku.edu.cn

Jin Zhang − *Beijing National Laboratory for Molecular Sciences, College of Chemistry and Molecular Engineering, Academy for Advanced Interdisciplinary Studies, Beijing Science and Engineering Center for Nanocarbons and School of Materials Science and Engineering, Peking University, Beijing 100871, China; Beijing Graphene Institute (BGI), Beijing 100095, China*; orcid.org/0000-0003-3731-8859; Email: jinzhang@pku.edu.cn

Authors

Xiangyang Li − *Beijing National Laboratory for Molecular Sciences, College of Chemistry and Molecular Engineering, Academy for Advanced Interdisciplinary Studies, Beijing Science and Engineering Center for Nanocarbons, Peking University, Beijing 100871, China; Beijing Graphene Institute (BGI), Beijing 100095, China*

Xudong Lei − *Institute of Mechanics, Chinese Academy of Sciences, Beijing 100190, China; School of Engineering Science, University of Chinese Academy of Sciences, Beijing 100049, China*

Xiangzheng Jia − *Department of Engineering Mechanics, School of Civil Engineering, Wuhan University, Wuhan 430072, China*

Tongzhao Sun − *Beijing Graphene Institute (BGI), Beijing 100095, China*

Xinyin Yang − *Beijing Graphene Institute (BGI), Beijing 100095, China*

Jiankun Huang − *Beijing Graphene Institute (BGI), Beijing 100095, China; School of Materials Science and Engineering, Peking University, Beijing 100871, China*

Xiaocang Han − *School of Materials Science and Engineering, Peking University, Beijing 100871, China*; orcid.org/0000-0001-8458-5568

Haolu Lin − *Beijing Graphene Institute (BGI), Beijing 100095, China*

Yunhang Li − *Beijing Graphene Institute (BGI), Beijing 100095, China*

Jiajun Luo − *Beijing National Laboratory for Molecular Sciences, College of Chemistry and Molecular Engineering, Academy for Advanced Interdisciplinary Studies, Beijing*

https://doi.org/10.1021/acsnano.5c14235
ACS Nano XXXX, XXX, XXX−XXX

Science and Engineering Center for Nanocarbons, Peking University, Beijing 100871, China

Xiaoxu Zhao − *School of Materials Science and Engineering, Peking University, Beijing 100871, China;* orcid.org/0000-0001-9746-3770

Enlai Gao − *Department of Engineering Mechanics, School of Civil Engineering, Wuhan University, Wuhan 430072, China;* orcid.org/0000-0003-1960-0260

Xianqian Wu − *Institute of Mechanics, Chinese Academy of Sciences, Beijing 100190, China; School of Engineering Science, University of Chinese Academy of Sciences, Beijing 100049, China;* orcid.org/0000-0001-5824-2203

Complete contact information is available at: https://pubs.acs.org/10.1021/acsnano.5c14235

Author Contributions

The manuscript was written through the contributions of all authors. All authors have given their approval to the final version of the manuscript.

Funding

The work was supported by the National Key Research and Development Program (2022YFA1203302 and 2022YFA1203304), the Beijing National Laboratory for Molecular Sciences (BNLMS202412 and BNLMS-CXTD-202001), the National Natural Science Foundation of China (52522202, 52202032, 52021006, T2188101, 12272391, 12232020), the Beijing Natural Science Foundation (2222094), the Strategic Priority Research Program of CAS (XDB36030100), the Shenzhen Science and Technology Innovation Commission (KQTD20221101115627004), the China Postdoctoral Science Foundation (2024M753316), the Postdoctoral Fellowship Program of CPSF (GZC20241782), and the CAS Project for Young Scientists in Basic Research (YSBR-096).

Notes

The authors declare no competing financial interest.

ACKNOWLEDGMENTS

We are grateful for the technical support for Nano-X from the Suzhou Institute of Nano-Tech and Nano-Bionics (SINANO), Chinese Academy of Sciences. The numerical calculations reported in this work were performed on the supercomputing system at the Supercomputing Center of Wuhan University.

REFERENCES

(1) Ritchie, R. O. The Conflicts between Strength and Toughness. *Nat. Mater.* **2011**, *10*, 817−822.

(2) Wegst, U. G. K.; Bai, H.; Saiz, E.; Tomsia, A. P.; Ritchie, R. O. Bioinspired Structural Materials. *Nat. Mater.* **2015**, *14*, 23−36.

(3) Nepal, D.; Kang, S.; Adstedt, K. M.; Kanhaiya, K.; Bockstaller, M. R.; Brinson, L. C.; Buehler, M. J.; Coveney, P. V.; Dayal, K.; El-Awady, J. A.; Henderson, L. C.; Kaplan, D. L.; Keten, S.; Kotov, N. A.; Schatz, G. C.; Vignolini, S.; Vollrath, F.; Wang, Y.; Yakobson, B. I.; Tsukruk, V. V.; et al. Hierarchically Structured Bioinspired Nanocomposites. *Nat. Mater.* **2023**, *22*, 18−35.

(4) Berglund, L. A.; Burgert, I. Bioinspired Wood Nanotechnology for Functional Materials. *Adv. Mater.* **2018**, *30* (19), 1704285.

(5) Yang, X.; Berglund, L. A. Structural and Ecofriendly Holocellulose Materials from Wood: Microscale Fibers and Nanoscale Fibrils. *Adv. Mater.* **2021**, *33* (28), 2001118.

(6) Xiao, S.; Chen, C.; Xia, Q.; Liu, Y.; Yao, Y.; Chen, Q.; Hartsfield, M.; Brozena, A.; Tu, K.; Eichhorn, S. J.; Yao, Y.; Li, J.; Gan, W.; Shi, S. Q.; Yang, V. W.; Lo Ricco, M.; Zhu, J. Y.; Burgert, I.; Luo, A.; Li, T.; et al. Lightweight, Strong, Moldable Wood Via Cell Wall Engineering As a Sustainable Structural Material. *Science* **2021**, *374*, 465−471.

(7) Hamedi, M. M.; Sandberg, M.; Olsson, R. T.; Pedersen, J.; Benselfelt, T.; Wohlert, J. Wood and Cellulose: the Most Sustainable Advanced Materials for Past, Present, and Future Civilizations. *Adv. Mater.* **2025**, *37* (22), 2415787.

(8) Zeng, G.; Dong, Y.; Luo, J.; Zhou, Y.; Li, C.; Li, K.; Li, X.; Li, J. Desirable Strong and Tough Adhesive Inspired by Dragonfly Wings and Plant Cell Walls. *ACS Nano* **2024**, *18*, 9451−9469.

(9) Bian, R.; Zhu, Y.; Lyu, Y.; Liu, Y.; Li, J.; Li, C.; Li, J. Bioinspired 'Phenol-Amine' Cross-Linking and Mineral Reinforcement Enable Strong, Tough, and Formaldehyde-Free Tannic Acid-Based Adhesives. *J. Clean. Prod.* **2024**, *472*, 143490.

(10) Li, C.; Zhao, Z.; Li, M.; Ye, Q.; Li, Z.; Wang, Y.; Peng, W.; Guo, J.; Chen, X.; Li, H. Constructing Ultra-Strong and Water Resistance Magnesium Oxychloride Cement-Based Adhesive for Wood Industry. *Adv. Compos. Hybrid Mater.* **2025**, *8*, 90.

(11) Yang, L.; Xing, M.; Xue, X.; Jin, X.; Wang, Y.; Xiao, F.; Li, C.; Wang, F. Preparation and Characterization of a Novel Eco-Friendly Acorn-Based Wood Adhesive with High Performance. *Forests* **2025**, *16*, 853.

(12) Chen, L.; Yu, L.; Qi, L.; Eichhorn, S. J.; Isogai, A.; Lizundia, E.; Zhu, J. Y.; Chen, C. Cellulose Nanocomposites by Supramolecular Chemistry Engineering. *Nat. Rev. Mater.* **2025**, *10*, 728−749.

(13) Yu, K.; Li, C.; Gu, W.; Wang, M.; Li, J.; Wen, K.; Xiao, Y.; Liu, S.; Liang, Y.; Guo, W.; Zhao, W.; Bai, J.; Ye, D.; Zhu, Y.; Zhu, M.; Zhou, X.; Liu, Z. High-Strength Cellulose Fibres Enabled by Molecular Packing. *Nat. Sustain.* **2025**, *8*, 411−421.

(14) Ling, S.; Kaplan, D. L.; Buehler, M. J. Nanofibrils in Nature and Materials Engineering. *Nat. Rev. Mater.* **2018**, *3*, 18016.

(15) Thomas, B.; Raj, M. C.; B, A. K.; H, R. M.; Joy, J.; Moores, A.; Drisko, G. L.; Sanchez, C. Nanocellulose, a Versatile Green Platform: From Biosources to Materials and Their Applications. *Chem. Rev.* **2018**, *118*, 11575−11625.

(16) Zhang, Y.; Yu, J.; Wang, X.; Durachko, D. M.; Zhang, S.; Cosgrove, D. J. Molecular Insights into the Complex Mechanics of Plant Epidermal Cell Walls. *Science* **2021**, *372*, 706−711.

(17) Bai, Y.; Yue, H.; Wang, J.; Shen, B.; Sun, S.; Wang, S.; Wang, H.; Li, X.; Xu, Z.; Zhang, R.; Wei, F. Super-Durable Ultralong Carbon Nanotubes. *Science* **2020**, *369*, 1104−1106.

(18) Zhang, X.; Lu, W.; Zhou, G.; Li, Q. Understanding the Mechanical and Conductive Properties of Carbon Nanotube Fibers for Smart Electronics. *Adv. Mater.* **2020**, *32* (5), 1902028.

(19) Chae, H. G.; Kumar, S. Making Strong Fibers. *Science* **2008**, *319*, 908−909.

(20) Smail, F.; Boies, A.; Windle, A. Direct Spinning of CNT Fibres: Past, Present and Future Scale Up. *Carbon* **2019**, *152*, 218−232.

(21) Lee, D.; Heo, S. J.; Kim, S. G.; Ku, B. C. A Review of High-Performance Carbon Nanotube-Based Carbon Fibers. *Funct. Compos. Struct.* **2023**, *5*, 045007.

(22) Guo, H.; Dong, C.; Han, Q.; Jiang, H.; Sun, H.; Sun, X.; Zhang, S.; Peng, H. Advancing Carbon Nanotube Fibers: Addressing Challenges from Production to Application. *ACS Central Sci.* **2025**, *11*, 855−867.

(23) Wu, K.; Zhang, Y.; Yong, Z.; Li, Q. Continuous Preparation and Performance Enhancement Techniques of Carbon Nanotube Fibers. *Acta Phys. -Chim. Sin.* **2022**, *38*, 2106034.

(24) Kim, S. G.; Choi, G. M.; Jeong, H. D.; Lee, D.; Kim, S.; Ryu, K. H.; Lee, S.; Kim, J.; Hwang, J. Y.; Kim, N. D.; Kim, D. Y.; Lee, H. S.; Ku, B. C. Hierarchical Structure Control in Solution Spinning for Strong and Multifunctional Carbon Nanotube Fibers. *Carbon* **2022**, *196*, 59−69.

(25) Wang, H.-Z.; Jiao, X.-Y.; Gao, Z.-Q.; Hou, P.-X.; Xu, L.-L.; Shi, C.; Liang, Y.; Wang, Y.-P.; Liu, C. Highly Conductive Double-Wall Carbon Nanotube Fibers Produced by Dry-Jet Wet Spinning. *Adv. Funct. Mater.* **2024**, *34* (39), 2404538.

(26) Lee, J.; Lee, D.-M.; Jung, Y.; Park, J.; Lee, H. S.; Kim, Y.-K.; Park, C. R.; Jeong, H. S.; Kim, S. M. Direct Spinning and

Densification Method for High-Performance Carbon Nanotube Fibers. *Nat. Commun.* **2019**, *10*, 2962.
(27) Bulmer, J. S.; Mizen, J. E.; Gspann, T. S.; Kaniyoor, A.; Ryley, J. B.; Kiley, P. J.; Sparkes, M. R.; O'Neill, B.; Elliott, J. A. Extreme Stretching of High G: D Ratio Carbon Nanotube Fibers Using Super-Acid. *Carbon* **2019**, *153*, 725−736.
(28) Zhang, X.; De Volder, M.; Zhou, W.; Issman, L.; Wei, X.; Kaniyoor, A.; Terrones Portas, J.; Smail, F.; Wang, Z.; Wang, Y.; et al. Simultaneously Enhanced Tenacity, Rupture Work, and Thermal Conductivity of Carbon Nanotube Fibers by Raising Effective Tube Portion. *Sci. Adv.* **2022**, *8*, No. eabq3515.
(29) Li, L.; Sun, T.; Lu, S.; Chen, Z.; Xu, S.; Jian, M.; Zhang, J. Graphene Interlocking Carbon Nanotubes for High-Strength and High-Conductivity Fibers. *ACS Appl. Mater. Interfaces* **2023**, *15*, 5701−5708.
(30) Niu, Y.; He, Z.; Wang, S.; Zhang, Y.; Yang, Z.; Zhang, Y.; Yong, Z.; Wu, K.; Zhao, L.; Guo, Z.; Jian, M.; Li, Q. Continuous Carbon Nanotube Fiber with an Extremely High Average Specific Strength of 4.1 $N{\cdot}tex^{-1}$. *Nano Res.* **2025**, *18*, 94907584.
(31) Xu, W.; Chen, Y.; Zhan, H.; Wang, J. N. High-Strength Carbon Nanotube Film from Improving Alignment and Densification. *Nano Lett.* **2016**, *16*, 946−952.
(32) Wu, K.; Wang, B.; Niu, Y.; Wang, W.; Wu, C.; Zhou, T.; Chen, L.; Zhan, X.; Wan, Z.; Wang, S.; Yang, Z.; Zhang, Y.; Zhang, L.; Zhang, Y.; Yong, Z.; Jian, M.; Li, Q. Carbon Nanotube Fibers with Excellent Mechanical and Electrical Properties by Structural Realigning and Densification. *Nano Res.* **2023**, *16*, 12762−12771.
(33) Shi, H. L.; Shi, Q. Q.; Zhan, H.; Ai, J. J.; Chen, Y. T.; Wang, J. N. High-Strength Carbon Nanotube Fibers from Purity Control by Atomized Catalytic Pyrolysis and Alignment Improvement by Continuous Large Prestraining. *Nano Lett.* **2023**, *23*, 10739−10747.
(34) Kim, S. G.; Heo, S. J.; Kim, S.; Kim, J.; Kim, S. O.; Lee, D.; Lee, S.; Kim, J.; You, N. H.; Kim, M.; Kim, H. C.; Chae, H. G.; Ku, B. C. Ultrahigh Strength and Modulus of Polyimide-Carbon Nanotube Based Carbon and Graphitic Fibers with Superior Electrical and Thermal Conductivities for Advanced Composite Applications. *Compos. Part B-Eng.* **2022**, *247*, 110342.
(35) Kim, J.; Heo, S. J.; Lee, D.; Im, B. W.; Kim, T. H.; Kim, S. G.; Ku, B. C. Highly Strong Carbon Fibers through Synergistic Carbonization Process of Sulfonated Poly(P-Phenylene Sulfide) and Carbon Nanotube. *Carbon* **2024**, *219*, 118814.
(36) Eo, S. B.; Lee, J.; Choi, J.; Son, H.; Lee, J. W.; Kim, S. S.; Lee, M. W.; Hwang, J. Y.; Kim, J.; Jeon, D. Y.; Moon, S. Y. Strengthening of Carbon Nanotube Fiber Using Ecofriendly Triblock Copolymer and Newly Designed Characterization Via Low-Frequency Noise. *Carbon* **2024**, *221*, 118894.
(37) Jang, J.; Park, K. T.; Lee, K.; Jung, Y.; Lee, J. I.; Kim, T. Enhancing the Mechanical Properties of CNTFibers through Alignment Control and Diazotization-Induced Crosslinking. *Appl. Surf. Sci.* **2025**, *706*, 163570.
(38) Jung, Y.; Cho, Y. S.; Park, J. H.; Cheon, J. Y.; Lee, J. W.; Kim, J. H.; Park, C. R.; Kim, T.; Yang, S. J. Selective Interbundle Cross-Linking for Lightweight and Superstrong Carbon Nanotube Yarns. *Nano Lett.* **2023**, *23*, 3128−3136.
(39) Huang, J.; Guo, Y.; Lei, X.; Chen, B.; Hao, H.; Luo, J.; Sun, T.; Jian, M.; Gao, E.; Wu, X.; Ma, W.; Shao, Y.; Zhang, J. Fabricating Ultrastrong Carbon Nanotube Fibers Via a Microwave Welding Interface. *ACS Nano* **2024**, *18*, 14377−14387.
(40) Beese, A. M.; Sarkar, S.; Nair, A.; Naraghi, M.; An, Z.; Moravsky, A.; Loutfy, R. O.; Buehler, M. J.; Nguyen, S. T.; Espinosa, H. D. Bio-Inspired Carbon Nanotube−Polymer Composite Yarns with Hydrogen Bond-Mediated Lateral Interactions. *ACS Nano* **2013**, *7*, 3434−3446.
(41) Boncel, S.; Sundaram, R. M.; Windle, A. H.; Koziol, K. K. K. Enhancement of the Mechanical Properties of Directly Spun CNT Fibers by Chemical Treatment. *ACS Nano* **2011**, *5*, 9339−9344.
(42) Zhang, X.; Lei, X.; Jia, X.; Sun, T.; Luo, J.; Xu, S.; Li, L.; Yan, D.; Shao, Y.; Yong, Z.; Zhang, Y.; Wu, X.; Gao, E.; Jian, M.; Zhang, J. Carbon Nanotube Fibers with Dynamic Strength up to 14 GPa. *Science* **2024**, *384*, 1318−1323.
(43) Chang, H.; Luo, J.; Gulgunje, P. V.; Kumar, S. Structural and Functional Fibers. *Annu. Rev. Mater. Res.* **2017**, *47*, 331−359.
(44) Park, J. H.; Rutledge, G. C. 50th Anniversary Perspective: Advanced Polymer Fibers: High Performance and Ultrafine. *Macromolecules* **2017**, *50*, 5627−5642.
(45) Hageman, J. C. L.; de Wijs, G. A.; de Groot, R. A.; Klop, E. A. The Role of the Hydrogen Bonding Network for the Shear Modulus of PIPD. *Polymer* **2005**, *46*, 9144−9154.
(46) Takahashi, Y. Crystal Structure of Poly(Pyridobisimidazole), PIPD. *Macromolecules* **2003**, *36*, 8652−8655.
(47) Wan, S.; Li, X.; Chen, Y.; Liu, N.; Wang, S.; Du, Y.; Xu, Z.; Deng, X.; Dou, S.; Jiang, L.; et al. Ultrastrong MXene Films Via the Synergy of Intercalating Small Flakes and Interfacial Bridging. *Nat. Commun.* **2022**, *13*, 7340.
(48) Wan, S.; Li, X.; Chen, Y.; Liu, N.; Du, Y.; Dou, S.; Jiang, L.; Cheng, Q. High-Strength Scalable MXene Films through Bridging-Induced Densification. *Science* **2021**, *374*, 96−99.
(49) Dai, H.; Chang, J.; Yang, J.; Wang, H.; Zhou, J.; Sun, G. Bio-Inspired Interfacial Engineering of MXene Fibers toward Synergistic Improvement in Mechanical Strength and Electrochemical Performance. *Adv. Funct. Mater.* **2024**, *34* (11), 2312654.
(50) Shahzadi, K.; Mohsin, I.; Wu, L.; Ge, X.; Jiang, Y.; Li, H.; Mu, X. Bio-Based Artificial Nacre with Excellent Mechanical and Barrier Properties Realized by a Facile In Situ Reduction and Cross-Linking Reaction. *ACS Nano* **2017**, *11*, 325−334.
(51) Woo, J. H.; Kim, N. H.; Kim, S. I.; Park, O. K.; Lee, J. H. Effects of the Addition of Boric Acid on the Physical Properties of MXene/Polyvinyl Alcohol (PVA) Nanocomposite. *Compos. Part B-Eng.* **2020**, *199*, 108205.
(52) Taylor, L. W.; Dewey, O. S.; Headrick, R. J.; Komatsu, N.; Peraca, N. M.; Wehmeyer, G.; Kono, J.; Pasquali, M. I. P. Increased Production, and the Path to Broad Adoption of Carbon Nanotube Fibers. *Carbon* **2021**, *171*, 689−694.
(53) Yan, D.; Luo, J.; Wang, S.; Han, X.; Lei, X.; Jiao, K.; Wu, X.; Qian, L.; Zhang, X.; Zhao, X.; et al. Carbon Nanotube-Directed 7 GPa Heterocyclic Aramid Fiber and Its Application in Artificial Muscles. *Adv. Mater.* **2024**, *36* (22), 2306129.
(54) Luo, J.; Wen, Y.; Jia, X.; Lei, X.; Gao, Z.; Jian, M.; Xiao, Z.; Li, L.; Zhang, J.; Li, T.; et al. Fabricating Strong and Tough Aramid Fibers by Small Addition of Carbon Nanotubes. *Nat. Commun.* **2023**, *14*, 3019.
(55) Wang, X.; Ho, V.; Segalman, R. A.; Cahill, D. G. Thermal Conductivity of High-Modulus Polymer Fibers. *Macromolecules* **2013**, *46*, 4937−4943.
(56) Kim, S. G.; Heo, S. J.; Kim, J.-G.; Kim, S. O.; Lee, D.; Kim, M.; Kim, N. D.; Kim, D.-Y.; Hwang, J. Y.; Chae, H. G.; et al. Ultrastrong Hybrid Fibers with Tunable Macromolecular Interfaces of Graphene Oxide and Carbon Nanotube for Multifunctional Applications. *Adv. Sci.* **2022**, *9* (29), 2203008.
(57) Gu, J.; Li, D.; Ren, Y.; Li, J.; Ji, X.; Liu, X.; Zhan, W.; Zhao, X.; Wang, Q.; Liu, X.; et al. Biomimetic Strong and Tough MXene Fibers with Synergy between Micropores and Dual Interfaces. *Nat. Commun.* **2025**, *16*, 9645.
(58) Li, P.; Wang, Z.; Qi, Y.; Cai, G.; Zhao, Y.; Ming, X.; Lin, Z.; Ma, W.; Lin, J.; Li, H.; et al. Bidirectionally Promoting Assembly Order for Ultrastiff and Highly Thermally Conductive Graphene Fibres. *Nat. Commun.* **2024**, *15*, 409.
(59) Newcomb, B. A. P. Structure, and Properties of Carbon Fibers. *Compos. Part A* **2016**, *91*, 262−282.
(60) Xiao, K.; Zhang, W.; Zhu, M.; Yin, Q.; Fortunelli, A.; Goddard, W. A., III; Wu, X. Dynamical Performance of Graphene Aerogel with Ductile and Brittle Characteristics. *Adv. Funct. Mater.* **2024**, *34* (29), 2401473.
(61) Portela, C. M.; Edwards, B. W.; Veysset, D.; Sun, Y.; Nelson, K. A.; Kochmann, D. M.; Greer, J. R. Supersonic Impact Resilience of Nanoarchitected Carbon. *Nat. Mater.* **2021**, *20*, 1491−1497.

https://doi.org/10.1021/acsnano.5c14235
ACS Nano XXXX, XXX, XXX−XXX

(62) Xie, W.; Tadepalli, S.; Park, S. H.; Kazemi Moridani, A.; Jiang, Q.; Singamaneni, S.; Lee, J. H. Extreme Mechanical Behavior of Nacre-Mimetic Graphene-Oxide and Silk Nanocomposites. *Nano Lett.* **2018**, *18*, 987−993.
(63) Kagias, M.; Lee, S.; Friedman, A. C.; Zheng, T.; Veysset, D.; Faraon, A.; Greer, J. R. Metasurface-Enabled Holographic Lithography for Impact-Absorbing Nanoarchitected Sheets. *Adv. Mater.* **2023**, *35* (13), 2209153.
(64) Xie, W.; Zhang, R.; Headrick, R. J.; Taylor, L. W.; Kooi, S.; Pasquali, M.; Müftü, S.; Lee, J. H. Dynamic Strengthening of Carbon Nanotube Fibers under Extreme Mechanical Impulses. *Nano Lett.* **2019**, *19*, 3519−3526.

https://doi.org/10.1021/acsnano.5c14235
ACS Nano XXXX, XXX, XXX−XXX